ELSEVIER

Thermochimica Acta 279 (1996) 65–76

thermochimica acta

Copper-zinc oxide catalysts. Part IV[1]. Thermal treatment in air, argon and hydrogen and XRD study of new bimetallic precursors–direct formation of alloys

Charles Kappenstein[a,*], Juraj Černák[a,2], Rachid Brahmi[a], Daniel Duprez[a], Jozef Chomič[b]

[a] *URA-CNRS 350, Equipe de Chimie Minérale, University of Poitiers, 40 Avenue du Recteur Pineau, 86022 Poitiers, France*

[b] *Department of Inorganic Chemistry, P.J. Šafárik University, Moyzesova 11, 041 54 Košice, Slovakia*

Received 16 June 1995; accepted 25 January 1996

Abstract

Four new Cu–Zn bimetallic precursors of model catalysts for methanolization of syngas, $Zn(NH_3)_2Cu(CN)_3$ (ZCA), $[Zn(\mathbf{en})_3]_6[Cu_5(CN)_{17}]\cdot nH_2O$ ($n = 8.4$) (ZCE3), $[Zn(\mathbf{en})][Cu(CN)_3]$ (ZCE1) and $[Zn_{1-x}Cu_x(\mathbf{en})][Cu(CN)_3]$ (ZCCE1), were thermally treated in air, hydrogen and argon atmosphere between 200 and 900°C. The calcinations in air yield firstly a mixture of cyano-ligand-containing compounds which transform at temperatures above 300°C to CuO and ZnO; the crystallite size of both oxides increases with temperature. The reduction in hydrogen at 300°C gives zinc cyanide and metallic copper which are converted at 450°C mainly to β'-brass including some α- and γ-alloys. The thermal treatment in argon displays the very high thermal stability of zinc cyanide to 900°C and formation of copper or α-CuZn alloy. Only the hydrogen treatment avoids the segregation of both metallic elements. The results are discussed on the basis of thermodynamic data.

Keywords: Argon; Bimetallic compounds; Catalyst precursors; Copper–zinc; Cyano complexes; Hydrogen; Thermal treatment

* Corresponding author. Fax: (33) 49 45 40 20; e-mail: kappenstein@zeus.univ-poitiers.fr

[1] For Part III, see R. [1]

[2] On leave from Department of Inorganic Chemistry, P.J. Šafárik University, Košice, Slovakia.

Elsevier Science B.V.
PII: S0040-6031(96)02869-9

1. Introduction

Generally, the preparation of Cu–ZnO catalysts for methanol synthesis involves the following steps [1]: (i) preparation of the precursor; (ii) calcination of the precursor; (iii) activation of the catalysts. The first step corresponds to the chemical synthesis of the appropriate precursor mainly by the coprecipitation method. The second step, calcination, involves the thermal decomposition of the appropriate precursor in air. This step normally leads to the formation of oxides with different structural and textural properties (crystallite size, surface area, etc.) depending on the calcination conditions and previous history of the precursor. The third step, activation, involves the reduction of CuO in hydrogen atmosphere to form catalytically active species.

These different stages of catalyst preparation have been studied extensively [2–4]. However, studies on the direct thermal decomposition in hydrogen atmosphere are scarce [5–8] although the reduction step in the catalyst preparation is an important part of the activation process. To our knowledge, no information concerning such thermal treatment of copper–zinc precursors appears in the open literature.

In our previous papers, we described the preparation, characterization and thermal properties under dynamic conditions of four Cu-Zn bimetallic compounds: $Zn(NH_3)_2Cu(CN)_3$ (ZCA), $[Zn(\mathbf{en})_3]_6[Cu_5(CN)_{17}]\cdot nH_2O$ ($n = 8.4$) (ZCE3), $[Zn(\mathbf{en})][Cu(CN)_3]$ (ZCE1) and $[Zn_{1-x}Cu_x(\mathbf{en})][Cu(CN)_3]$ (ZCCE1) [9]. The crystal structures of ZCA and ZCE3 have been described [10].

The aim of the present work is to characterize the products obtained after thermal treatment of these bimetallic compounds at different temperatures and in different atmospheres. The crystalline phases were identified by powder X-ray diffractometry (XRD) whereas we used FTIR spectroscopy for the characterization of amorphous products.

2. Experimental

The studied compounds (ZCA), (ZCE3), (ZCE1) and (ZCCE1) were prepared as described in Ref. [9].

2.1. Phase analyses

Phase analyses were carried out on a computerized Siemens D-500 Kristalloflex diffractometer. Cu Kα radiation back-monochromatized by a graphite monochromator was used ($\lambda\,K\alpha_1 = 1.54060$ Å). The diffractograms were recorded in step mode (0.02–0.04°, 1 s). The present phases were identified by use of the JCPDS library (PDF) [11] and the SEARCH program (Socabim, France). Data handling was carried out using the software package EVA and FIT (Socabim, France). The size of the crystallites for CuO and ZnO phases were determined from the integral width β (area/height) of the different peaks using the Williamson–Hall relation [12]: $\beta\cos\theta = (\lambda/D) + 4\varepsilon\sin\theta$, where θ is the Bragg angle, D the mean size in volume of the crystallites, ε the strain and β the corrected integral width.

2.2. *Infrared spectroscopy*

Infrared spectra were recorded as KBr pellets (1–2% of sample in weight) on a Nicolet 510 FT–IR apparatus in the region from 4000 to 400 cm^{-1}. The intensity of the peaks is labelled as follows: vs, very strong; s, strong; m, medium; sh, shoulder; w. weak.

2.3 *Calcination*

The thermal treatments in air, hydrogen and argon atmospheres were carried out in isothermal conditions using programmable furnaces. The sample weights were in the range 150–250 mg. For calcinations in air, a horizontal furnace was used with the sample placed in a quartz boat, thus leading to weight loss determination. The thermal treatments in hydrogen and argon atmospheres were performed in a vertical furnace by using glass or quartz U-shaped reactors. As the volatile decomposition products condensed in colder parts of the reactor, only identification of the products was carried out. The heating rate was 4°C min^{-1} and the samples were kept for 3 h at the final temperature between 200 and 900°C. The flow rate of hydrogen and argon was 30 cm^3 min^{-1}.

3. Results and discussion

3.1. *Calcination in air*

The X-ray diffractograms of the calcination products of ZCA obtained at different temperatures are collected in Fig. 1. The calcination at 200°C yields an amorphous product (weight loss 16.2%, calc. 14.3% for two molecules of ammonia). The IR spectrum displays three ν(CN) peaks at 2218 m, 2174 sh and 2157 vs cm^{-1}; the first one may correspond to bridging cyano ligands present in $Zn(CN)_2$ (ν(CN) at 2225 cm^{-1}, Ref. [13]), whereas the two others may suggest the presence of $ZnCu_2(CN)_4$ from stoichiometric considerations. The formation of $Zn(CN)_2$ means that at least some of the cyano groups have changed their coordination mode, as can be deduced from knowledge of the crystal structure [14]. This process should involve the breaking of the initial Zn—N bond, rotation of the CN group and formation of a new Zn—C bond.

The calcination at 300°C yields a mixture of ZnO (36-1451, zincite), CuO (41-254, tenorite) (major phases), Cu (4-836) and Cu_2O (5-667, cuprite) (minor phases) [11]. The simultaneous presence of copper and both oxides, which is not possible from a thermodynamic point of view, indicates the macroscopic heterogeneity of the sample. The observed weight loss, 35.0%, lies between the values calculated for the presence of Cu + ZnO (39.9%) and CuO + ZnO (33.2%). The increase in the calcination temperature produces a mixture of the respective oxides CuO and ZnO (Cu_2O was still detected at 450°C). At the same time the crystallite size of both oxides increases with temperature, thus indicating a sintering process: size/Å (T/°C) 220 (450), 310 (600), 430 (900) for

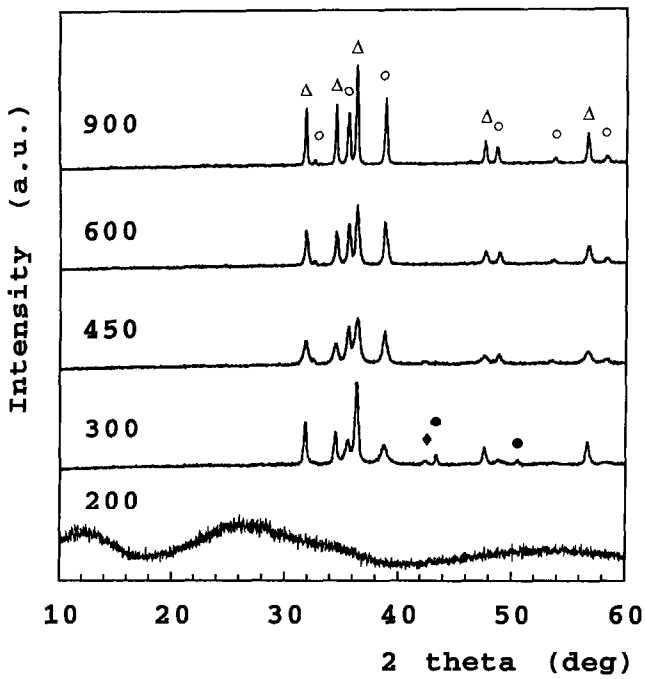

Fig. 1. XRD patterns for ZCA calcinated in air at different temperatures which are given on the figure in °C. The intensity scale for the diffractogram at 200°C is ten times smaller than for the others. The observed phases are indicated as follows: Δ, ZnO; ○, CuO; ●, Cu; ◆, Cu_2O.

CuO; and 190 (450), 250 (600), 560 (900) for ZnO. The average observed weight loss (34.3%) is in agreement with the formation of oxides (calc. 33.2%).

The product of the calcination of ZCE3 at 200°C contains poorly crystallized $Zn(CN)_2$ and another unidentified phase (Fig. 2). The IR spectrum corroborates the presence of $Zn(CN)_2$ (2218w cm^{-1}) and compound(s) containing cyano groups (2143vs cm^{-1}) and remaining **en** ligands (peaks at 3312m, 1601w, 1125m, 1001m, 613m cm^{-1}). The observed weight loss of 47.1% is lower than the value calculated for the departure of all **en** ligands (51.7%) thus disclosing their presence.

The calcination at 300°C yields $Zn(CN)_2$ as the major crystalline phase (strong IR peak at 2218 cm^{-1}) and traces of Cu and ZnO can be observed. Thus the copper is present as a major amorphous phase containing cyano ligands as revealed by the IR peaks at 2168 ssh and 2140 s cm^{-1}. The first peak is in agreement with poorly crystallized copper cyanide CuCN (2172 cm^{-1}, Ref. [13]). From 450 to 900°C, the calcinations yield mixtures of CuO and ZnO and the crystallite size increases with temperature: 180 to 410 Å for CuO, and 150 to 550 Å for ZnO. The observed weight losses between 450 and 900°C are in the range 63.3–64.4%; the calculated value for CuO and ZnO is 62.9%.

Fig. 3 displays the diffraction pattern for the calcination products of ZCE1 and ZCCE1 at 300 and 450°C and both compounds behave similarly. Upon calcination at

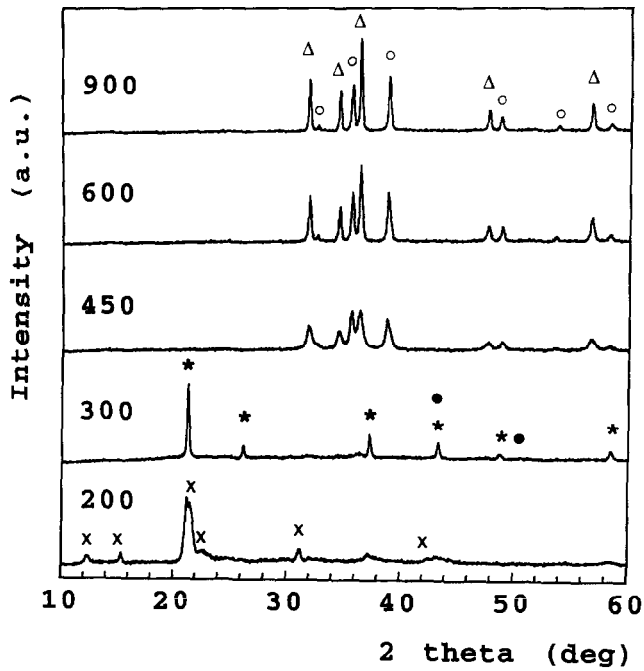

Fig. 2. XRD pattern for ZCE3 calcinated in air at different temperatures which are given on the figure in °C. The observed phases are indicated as follows: Δ, ZnO; ○, CuO; ●, Cu; ⋆, $Zn(CN)_2$; x, unidentified phase.

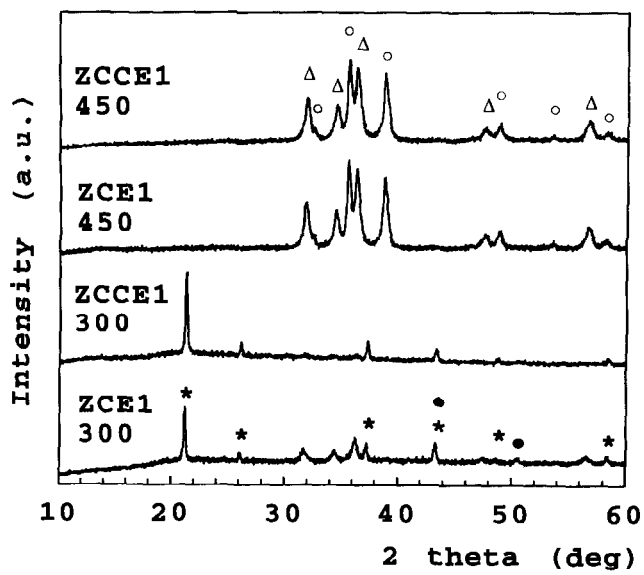

Fig. 3. XRD pattern for ZCE1 and ZCCE1 calcinated in air at different temperatures which are given on the figure in °C. The observed phases are indicated as follows: Δ, ZnO; ○, CuO; ●, Cu; ⋆, $Zn(CN)_2$.

300°C the formation of $Zn(CN)_2$ was clearly in evidence and the presence of ZnO can be observed for ZCE1 as well as traces of copper. At 450°C, both compounds yield mixtures of CuO and ZnO with the same crystallite size as for ZCE3: 190 Å for CuO, and 140 Å for ZnO. The observed weight loss is 40.9% (calc. 39.7%).

Zinc cyanide $Zn(CN)_2$ is the major crystalline intermediate during air decomposition and its formation is in line with the high stability (decomposition temperature: 800°C, Ref. [15]). In our case it was already decomposed at 450°C (300°C for ZCA) in air and this observation could be explained by the catalytic behaviour of metallic copper [16]. Such metallic copper was clearly observed at 300°C in our samples and its formation can be explained by internal redox reactions between Cu(I) and cyano ligands inside the bulk of the sample. This copper is further reoxidized to CuO via Cu_2O. However, the Cu(I) in contact with air may be directly oxidized to CuO.

3.2. *Calcination in hydrogen*

The precursors were heated in hydrogen flow at 300 and 450°C (or 500°C). The heating of ZCA and ZCE3 at 300°C yields zinc cyanide and metallic copper as the main phases, thus indicating segregation of both metallic elements and participation of hydrogen in this process (Fig. 4). In the case of ZCE1, the calcination at this temperature leads to the same mixture along with the unidentified phase previously found after the calcination of ZCE3 in air at 200°C. This different behaviour is probably due to higher thermal stability of the intermediate(s) formed during calcination. The weight loss cannot be determined precisely as the volatile products condensed on the colder parts of the U-shaped reactor.

The hydrogen participation in the reduction of zinc cyanide is clearly evidenced by the formation of brass alloys after calcination at 450°C (Fig. 5). The experimental values of weight loss were in line with the values calculated for the formation of

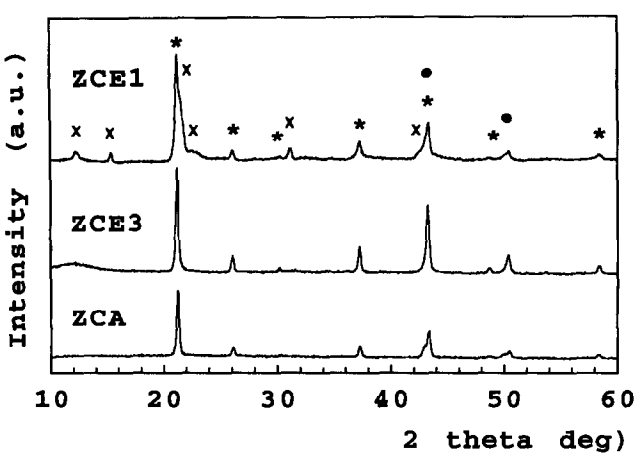

Fig. 4. XRD pattern for compounds heated in hydrogen flow at 300°C. The observed phases are indicated as follows: ●, Cu; ⋆, $Zn(CN)_2$; x, unidentified phase.

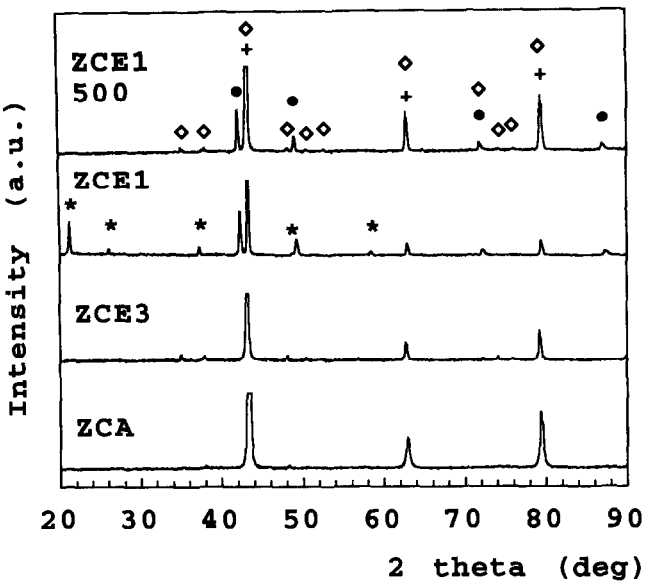

Fig. 5. XRD pattern for compounds heated in hydrogen flow at 450 (500)°C. The peaks exhibiting highest intensities were cut to show the low intensity peaks. The observed phases are indicated as follows: ●, α-CuZn; +, β′-CuZn; ◇, γ-CuZn; ⋆, $Zn(CN)_2$.

Cu + Zn, given in parentheses: ZCA, 54.1% (53.5%); ZCE3, 70.6% (70.2%); ZCE1, 53.0% (51.7%). The higher discrepancy between experimental and calculated values of ZCE1 can be explained by the presence of residual $Zn(CN)_2$ (Fig. 5).

The diffractogram of the calcination product of ZCA at 450°C display three strong peaks (Fig. 5) (lattice spacing: 2.086, 1.476 and 1.206 Å) and some peaks of very low intensity ($I_r = 0.2–1.0\%$). The position of the strong peaks corresponds to the strong reflections of the β′- and γ-Cu-Zn alloys, Zhanghengite, β′-CuZn phase (2-1231) and γ-Cu_5Zn_8 phase (25-1228). The position of the low intensity peaks agrees only with the γ-phase but their relative intensities are much lower than expected, whereas the weak reflections given on the card corresponding to the β′-phase are not observed.

The ideal structure of Zhanghengite (CuZn, low-temperature phase) is the ordered CsCl structure type. The high-temperature β-phase with transition temperature about 460°C [17] forms a disordered bcc unit cell; this phase is not present in the JCPD File [11]. The PDF card of the β′-phase gives the intensities of the peaks based on the ordered low-temperature structure; they have been measured using GaKα radiation (not given on the card, see Ref. [18]) which, due to anomalous dispersion, is the most favourable for observation of weak superstructure reflections ($h + k + l = 2n + 1$) of the ordered structure [18]. In the case of the CuKα radiation, the difference between the ordered and disordered phases cannot be observed; a model calculation using the program XQPA92 [19] has shown an intensity ratio of 1/4000 for the (100) and (110) reflections, which is not attainable in our conditions.

The positions and intensities of the three above-mentioned strong peaks correspond well to the reflection with $h+h+l=2n$ of Zhanghengite if we take into consideration the use of less favourable CuKα radiation. The Cu–Zn phase diagram [17] shows that for a Cu:Zn atomic ratio of 1:1, the alloy corresponds to a mixture of β'- or β- and γ-phases. On the basis of this information we assume that the calcination product is formed by major β'-CuZn phase and minor γ-Cu_5Zn_8 phase. A similar conclusion can be adopted for the calcination product of ZCE3 for which the peaks corresponding to the γ-alloy are somewhat more intense as in the case of ZCA. This is in line with the initial 5:6 Cu:Zn ratio in this compound.

The presence of zinc cyanide as a minor phase was still observed in the calcination product of ZCE1 at 450°C along with the β'-alloy (Zhanghengite, 2-1231) as the main product. The superfluous copper (as part of the zinc is bonded in zinc cyanide) is present as an α-phase. Its zinc content was estimated from the lattice parameter shift [20] ($a=3.697$ Å) to be approximately 36.7% in weight. The zinc cyanide disappears after calcination at 500°C, and γ-Cu_5Zn_8 is present along with some α-alloy containing 41.9% zinc ($a=3.710$ Å), which corresponds approximatively to the limit of zinc solubility [17]. As the intensities of the "weak" peaks of γ-Cu_5Zn_8 are roughly halved when compared with the tabulated values (with regard to the most intense peak), we assume the presence of Zhanghengite in the calcination product as well (see previous discussion). The presence of these different phases can be explained by the macroscopic heterogenity of the sample.

3.3. Calcination in argon

To avoid the possibility of the compounds reacting with the surrounding atmosphere, the thermal treatments were also carried out in argon.

The diffractograms of the products after calcination of ZCA in argon are shown in Fig. 6. At 300°C the X-ray measurement indicates the presence of $Zn(CN)_2$ and another unidentified phase. The IR spectrum displays the medium ν(CN) peak assigned to the zinc cyanide (2218 m cm^{-1}) and a strong peak with a shoulder (2157 vs and 2174 ssh cm^{-1}) presumably due to the double cyanide $ZnCu_2(CN)_4$ (see above). A similar IR spectrum was obtained after the calcination of ZCA in air at 200°C but in this case the product was amorphous. From the peak position of the unidentified phase it was possible to index the reflections (program DICVOL, Ref. [21]) in the tetragonal system. The cell parameters were refined using the program LSUCRIPC 22] ($a=12.60(1)$ Å, $c=4.924(1)$ Å; see Table 1).

$Zn(CN)_2$ becomes the major phase in the calcination product at 450°C along with another unidentified minor phase (lattice spacings 3.544, 3.007 and 2.188 Å) which could contain copper.

The product after heating ZCA at 600°C is a mixture of $Zn(CN)_2$ and metallic copper ($a=3.616$ Å). The diffractogram also contains the three peaks corresponding to the same phase already found at 450°C. The very high stability of $Zn(CN)_2$ in this neutral atmosphere is confirmed after thermal treatment at 900°C for 3 h, as it always remains the major phase (Fig. 6). Nevertheless, a part of the zinc was reduced and is present in

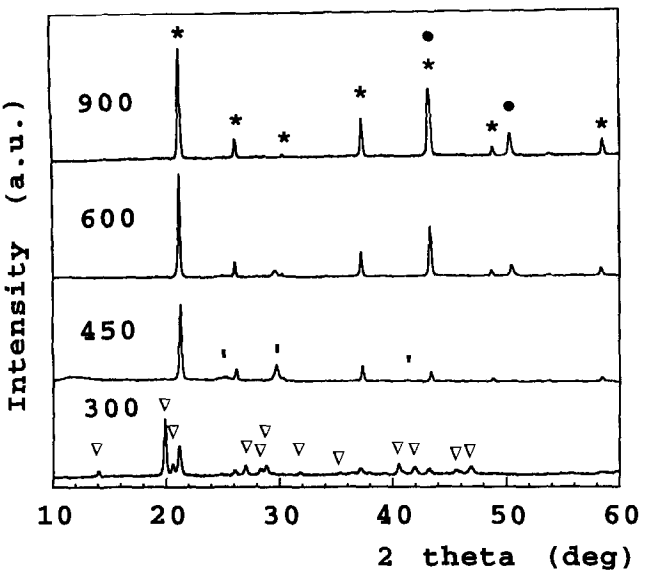

Fig. 6. XRD pattern for ZCA heated in argon at different temperatures which are given in the figure in °C. The observed phases are indicated as follows: ●, Cu or α-CuZn; ★, $Zn(CN)_2$; ∇, $ZnCu_2(CN)_4$; I, unidentified phase.

Table 1
XRD powder data for the product of ZCA heating in argon at 300°C ($ZnCu_2(CN)_4$)·($\lambda = 1.540598$ Å). The relative intensities are derived from the height of the peaks. Refined cell parameters are: $a = 12.60(1)$ Å, $c = 4.924(1)$ Å, $V = 781(1)$ Å^3

h	k	l	I/I_0	$2\theta_{cal}$	$2\theta_{obs}$	$\Delta 2\theta$
2	0	0	15	14.048	14.020	.028
2	2	0	100	19.917	19.915	.002
1	1	1	26	20.594	20.565	.029
2	2	1	16	26.971	26.963	.008
4	0	0	17	28.312	28.326	−.014
3	1	1	24	28.803	28.785	.018
4	2	0	14	31.737	31.729	.008
3	3	1	12	35.267	35.299	−.032
5	1	0	13	36.330	36.319	.011
1	1	2	13	37.886	37.885	.001
4	4	0	27	40.469	40.483	−.014
2	2	2	21	41.895	41.894	.001
6	2	0	16	45.497	45.487	.010
4	0	2	21	46.799	46.816	−.017

the Cu-Zu α-phase (about 5.7% in weight from the lattice parameter shift, $a = 3.628$ Å); the presence of metallic Zn in the colder part of the reactor is also observed.

The heating of the **en**–containing compound ZCE3 at 300°C in argon yielded the same products as the thermal treatment in hydrogen at the same temperature (Fig. 7,

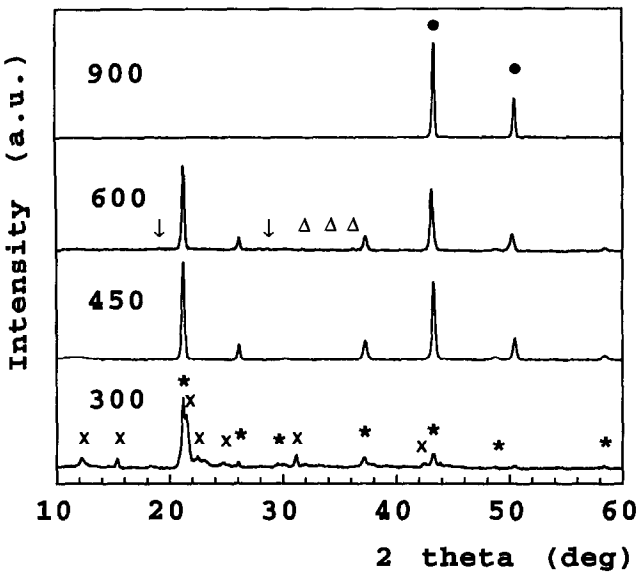

Fig. 7. XRD pattern for ZCE3 at different temperatures which are given in the figure in °C. The observed phases are indicated as follows: ●, Cu or α-CuZn; ⋆, $Zn(CN)_2$; Δ, ZnO; ↓, $ZnCN_2$; x, unidentified phase.

compare with Fig. 4). Further heating in argon at 450°C led to a mixture of $Zn(CN)_2$ and metallic Cu ($a = 3.618$ Å). This is in line with the high thermal stability of $Zn(CN)_2$ in argon and with internal redox reactions leading to the formation of copper metal.

At 600°C, we observe the formation of an α-alloy of zinc in copper ($a = 3.633$ Å; 8.3% of Zn), indicating the transformation of a small part of zinc cyanide. Moreover, the diffractogram discloses the presence of very small peaks of zinc cyanamide (1-788) and zinc oxide. The presence of ZnO in traces was confirmed in a repeated experiment and can be explained by oxygen impurities in argon (of the order of 0.1 ppm). The presence of zinc cyanamid may be the consequence of the action of a trace of oxygen on zinc cyanide.

The temperature increase to 900°C resulted in zinc segregation due to the vaporization of the Zn phase: it was present on the colder parts of the reactor as a zinc mirror. The remaining solid was identified as metallic copper ($a = 3.618$ Å). The experiments with ZCE1 were carried out only up to 450°C as they gave the same results as for ZCE3.

The stability of $Zn(CN)_2$ seems to play a key factor for the formation of products at high temperature under inert atmosphere when we compare the ammonia- and **en**-containing compounds.

On the basis of thermodynamic data, we can estimate the temperatures corresponding to the sign inversion of Gibbs energy variation (inversion temperature) with the aim of obtaining information about the thermodynamic possibility of different decomposition paths of zinc cyanide. The enthalpies and entropies for the different reactants and products were taken from Refs. [15a, 20]; the enthalpy of formation of $Zn(CN)_2$ was

found in Ref. [15b] (77 kJ mol^{-1}) and the entropy was estimated by comparison with CuCl, CuCN and $ZnCl_2$ (110 J K^{-1} mol^{-1}). The results for the decomposition reactions in the different gas flows are ($\Delta_r H°$/kJ mol^{-1}; $\Delta_r S°$/J K^{-1} mol^{-1}; T_i/°C)

$$Zn(CN)_2(s) + 5/2\,O_2(g) = ZnO(s) + 2\,CO_2(g) + N_2(g) \quad (-1216; 42; -)$$

$$Zn(CN)_2(s) + H_2(g) + Cu(s) = \beta'\text{-}CuZn(s) + 2\,HCN(g) \quad (172; 207; 560)$$

$$Zn(CN)_2(s) = Zn(g) + (CN)_2(g) \quad (361; 293; 959)$$

The decomposition is clearly favoured under oxidative conditions ($\Delta_r G° < 0$, whatever the temperature) with formation of zinc oxide which is already found at 300°C. Under hydrogen, the possibility of alloy formation favours the decomposition when compared to the formation of pure zinc [20]. Under argon, the inversion temperature is very high, in line with our experimental observation.

4. Conclusions

Whatever the nature of the gas flow, the thermal treatment resulted firstly in the formation of metallic copper and zinc cyanide as the main or rexclusive products. This indicates segregation of both metallic elements present in the precursor. The next step depends on the nature of the atmosphere, as hydrogen or oxygen takes part in the decomposition reactions: (i) formation of oxides in air; (ii) formation of alloys under hydrogen at low temperature; (iii) formation of metals or alloys at higher temperature. The very high thermal stability of zinc cyanide under argon was noticed.

In the presence of oxygen, zinc cyanide is directly oxidized to ZnO, preventing the formation of alloys. It decomposes at low temperature due to the catalytic action of the formed copper.

The formation of different Cu–Zn alloys in powdered form during calcination in hydrogen is the consequence of the primary reduction of zinc cyanide by hydrogen at rather low temperatures. The nature of the alloy phases (α-, β'- and γ-phases) is clearly related to the initial Cu/Zn atomic ratio. The mechanism of brass formation from the mixture of $Zn(CN)_2$ and metallic copper is favoured by the low melting point of zinc (420°C) and by the reduction of zinc cyanide under hydrogen. If, for simplicity, we take as a product the β'-alloy, the possible reactions are

$$Cu(s) + x\,Zn(CN)_2(s) + x\,H_2(g) = CuZn_x(\alpha, s) + 2x\,HCN(g)$$

$$CuZn_x(\alpha, s) + (1 - x)Zn(CN)_2(s) + (1 - x)\,H_2(g) = CuZn(\beta, s) + (2 - 2x)\,HCN(g)$$

Under argon, we can observe only the formation of the α-phase at higher temperature, as the formation of intermediate metallic zinc needs the decomposition of zinc cyanide. This decomposition reaction is not thermally favoured and needs a higher temperature for which the partial pressure of zinc vapour is significant, thus leading in dynamic conditions of gas flow to the departure of zinc from the reaction mixture.

Acknowledgements

This research was carried out in the framework of Slovak-French scientific cooperation. The financial support from the Slovak Ministry of Education and Sciences (grant No. 1445/94) is acknowledged. One of us (J.Č.) thanks the University of Poitiers for its support.

References

[1] J. Černák, C. Kappenstein, Z. Žák and J. Chomič, Acta Crystallogr., Sect. C52 (1996) to be published.
[2] G.C. Chinchen, P.J. Denny, J.R. Jennings, M.S. Spencer and K.C. Waugh, Appl. Catal., 36 (1988) 1.
[3] P. Porta, S. De Rossi, G. Ferraris and F. Pompa, Solid State Ionics, 45 (1991) 34.
[4] D. Waller, D. Stirling and F.S. Stone, Faraday Discuss. Chem. Soc., 87 (1989) 107.
[5] S. Kanda, T. Kori and S. Kida, J. Solid State Chem., 108 (1994) 299.
[6] S. Aschwanden, H.W. Schmalle, A. Reller and H.R. Oswald, Mater. Res. Bull., 28 (1993) 45.
[7] V.N. Pichkov, N.M. Sinitsyn, B.E. Stul'pin and L.K. Shubochkin, Zh. Neorg. Khim., 34 (1989) 536.
[8] J. Yuan, X. Xin and A. Dai, Thermochim. Acta, 130 (1988) 77.
[9] J. Černák, J. Chomič, C. Kappenstein, R. Brahmi and D. Duprez, Thermochim. Acta, 276 (1996) 209.
[10] J. Černák, C. Kappenstein, J. Chomič and M. Dunaj-Jurčo, Z. Krist., 209 (1994) 430.
[11] X-ray Powder Data File: 1-788 for $ZnCN_2$; 2-1231 for Zhanghengite, CuZn; 4-836 for Cu; 6-175 for $Zn(CN)_2$; 25-1228 for γ-copper zinc, Cu_5Zn_8; 36-1451 for zincite, zinc oxide; 41-254 for tenorite, CuO. JCPDF, USA, 1994.
[12] G.K. Williamson and W.H. Hall, Acta Metall., 1 (1953) 22.
[13] A.G. Sharpe, The Chemistry of Cyano Complexes of the Transition Metals, Academic Press, London, 1976.
[14] B.F. Hoskins and R. Robson, J. Am. Chem. Soc., 112 (1990) 1546.
[15] CRC Handbook of Physics and Chemistry: (a) 73th edn., CRC Press, Boca Raton, USA, 1993; (b) 62th edn., 1982.
[16] V. Ruml, Tagungsband-Kammer Tech. Suhl, 53 (1979) 87; Chem. Abst., 95 120540j.
[17] G. Pomey, Métallurgie, Techniques de del'Ingénieur, Paris, 1990.
[18] H. Nowotny and A. Winkels, Z. Phys. 114 (1939) 455.
[19] L. Smrcok and Z. Weiss, J. Appl. Crystallogr., 26 (1993) 140.
[20] C.J. Smithless (Ed.), Metals Reference Book, 5th edn., Butterworths, London, 1976.
[21] A. Boultif and D. Louer, J. Appl. Crystallogr., 24 (1991) 987.
[22] R.G. Garvey, Powder Diffr., 1 (1986) 114.